Formation of limit-periodic structures by quadrupole particles confined to a triangular lattice

David M. Rutkowski, Catherine Marcoux, Joshua E. S. Socolar, and Carol K. Hall

Phys. Rev. E **95**, 012604 — Published 10 January 2017

DOI: 10.1103/PhysRevE.95.012604

Formation of limit-periodic structures by quadrupole particles confined to a triangular lattice

David M. Rutkowski[a], Catherine Marcoux[b], Joshua E. S. Socolar[b] and Carol K. Hall*[a]

a- Department of Chemical & Biomolecular Engineering, North Carolina State University, Raleigh, North Carolina 27606, USA

b- Physics Department, Duke University, Durham, North Carolina 27708, USA

* hall@ncsu.edu

ABSTRACT

We have performed Monte Carlo (MC) simulations on two-dimensional systems of quadrupole particles confined to a triangular lattice in order to determine the conditions that permit the formation of a limit-periodic phase. We have found that limit-periodic structures form only when the rotations of the particles are confined to a set of six orientations aligned with the lattice directions. Related structures including striped and unidirectional rattler phases form when $\pi/6$ rotations or continuous rotations are allowed. Order parameters signaling the formation of the limit-periodic structure and related structures are measured as a function of temperature. Our findings on the formation of the limit-periodic structure elucidate features relevant to the experimental creation of such a structure, which is expected to have interesting vibrational and electromagnetic modes.

I. BACKGROUND AND INTRO

Nonperiodic structures with long range order are of interest both theoretically and experimentally due to their novel (expected or observed) electronic, photonic, elastic and frictional properties [1]. Since the discovery of quasicrystals in the 1980's the definition of the term "crystal" has changed to include nonperiodic structures, and now refers to any structures with sharp diffraction peaks indicating long-ranged translational order [2]. The possibility of having equilibrium phases exhibiting perfect translational order without the regular, periodic repetition of a unit cell is now well established [2].

Quasicrystals are non-periodic structures that have point group symmetries that are incompatible with periodicity, meaning they have diffraction patterns indicating symmetries not found in crystals (e.g. 8, 10, or 12-fold rotational symmetry in 2D or icosahedral symmetry in 3D). The earliest examples of quasicrystals were metallic made from binary or ternary metals typically involving the element aluminum [3]. More recently nonmetallic quasicrystals have been created with liquid crystals [4], ABC-star polymers [5], colloidal particles [6] and inorganic nanoparticles [7,8]. Metallic quasicrystals have been found or envisioned for use as non-stick heat insulation replacing Teflon, mechanical reinforcement, corrosion resistant surfaces and as hydrogen storage materials [9] while nonmetallic quasicrystals are expected to be useful in photonic applications [10].

Limit-periodic structures, like quasicrystals, are homogeneous, nonperiodic structures with long range order; however, unlike quasicrystals they consist of a union of periodic structures with ever-increasing lattice constants, $\xi^n a$, where ξ is an integer scale factor and $n = 1,...\infty$. Each periodic subset of the limit-periodic structure is referred to as a "level". The structure with the smallest lattice constant is level-1, the structure with the next largest lattice constant is level-2, and so on. There is no largest lattice constant defining a unit cell for the full

structure, hence the system is nonperiodic. The limit periodic structure would be recognizable from its diffraction pattern, which has a crystallographic point group symmetry but consists of a dense set of Bragg peaks at wavevectors $\xi^{-n}\sum m_i \boldsymbol{b}_i$ for $n \to \infty$ and all integers m_i, where the $\boldsymbol{b}_i$ are the basis vectors of the reciprocal lattice associated with level 1 alone. For the systems considered here, the periodic subsets comprising the structure have densities that scale like ξ^{-2n}, which is reflected in the fact that peak amplitudes decay exponentially with n for $m_i = \delta_{ij}$ with any j. An example of a limit-periodic structure and its diffraction pattern can be seen in the work by Byington and Socolar in which kagome lattices of increasing size overlap to form a single limit-periodic structure [1,11]. Such structures have been shown to be ground states of systems with physically plausible Hamiltonians and have been observed to form through a sequence of phase transitions in simulations of slow cooling from a random initial state in several models [1,11,12]. To date, however, no experimental realization of an equilibrium or self-assembled limit-periodic structure has been reported.

The simplest demonstrations of the possibility of limit-periodic ground states are framed in the language of tiling theory. It has been shown that limit-periodic structures are the only space-filling, non-overlapping arrangements of certain types of tiles endowed with appropriate matching rules for the relative orientations of adjacent tiles. Each type of tile in a given aperiodic set is called a prototile and may be characterized by its shape alone or by decorations that specify its type and orientation. Prototiles that force limit-periodic tilings have been constructed by Berger [13], Robinson [14], Goodman-Strauss [15], and by Socolar and Taylor [1,16]. The latter is of particular interest because only a single prototile (and its symmetry-related partners) is required.

Remarkably, as has recently been shown, strict matching rules specifying limit-periodicity are not required for the formation of limit-periodic structures. Marcoux et al. found that a simplified version of the model investigated by Socolar and Taylor can lead to a limit-periodic structure upon slow reduction of the temperature even though it has a periodic ground state [11]. This simplification is called the "black stripe model" and consists of a hexagonal prototile with lines decorating its surface to indicate which neighboring orientations are favored (Fig. 1a). If the black segments on two tiles sharing an edge are continuous across that edge, the interaction energy is taken to be zero, while a positive energy is assigned to edges where the black lines do not meet. The black-stripe decoration of the hexagonal prototile, along with the energy penalties described above, turns out to induce the formation of a limit-periodic structure even though there exist degenerate ground states that are periodic.

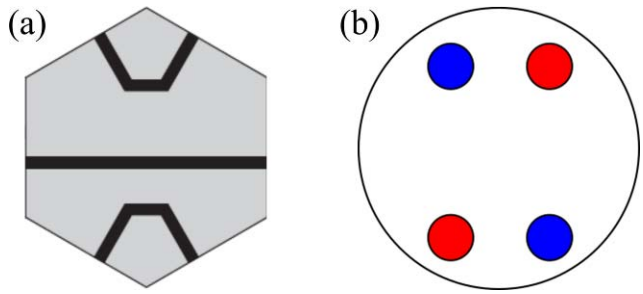

FIG. 1. (a) Black-stripe model in which the specific pattern of lines induces the formation of a limit-periodic structure upon slow temperature quench [11]. (b) Quadrupole disk model with four charges of alternating sign. The charges in play a similar role to the top and bottom lines in (a); the horizontal bar in (a) is however absent in (b).

The model considered in this paper, shown in Fig 1b and termed the "quadrupole disk model," mimics some of the crucial features of the black-stripe model. In this image, red circles (circles located at the northeast and southwest of the disk) represent positive charges while blue circles (circles located at the northwest and southeast of the disk) represent negative charges. There is a repulsive interaction (and therefore an energy penalty) when charges of like sign are near each other, while there is an attractive interaction when charges of unlike sign are near each

other. These charges act to mimic the matching rules for the short segments near the top and bottom of the black stripe prototile. A key difference between the present model and the black-stripe model, however, is that the long stripe linking opposite edges of the hexagonal prototile, which is offset from the tile center, is not represented at all by the charge distribution; in this sense our model is a simplification of the black-stripe model, and formation of a limit-periodic phase in our model demonstrates a greater degree of robustness of the limit-periodic phase than previously reported.

Quadrupolar disks could potentially be created from anisotropic colloidal particles. For example, colloidal particles with a small metallic patch on their surface have been shown to have quadrupolar interactions under the influence of an external electric field at high frequency [17-19]. These particles served as branching points in a mixture of dipolar and quadrupolar colloids. Additionally, colloids embedded in a nematic liquid crystal have been found to have quadrupole-like interactions allowing them to form square lattices. These particles were shown to be at least metastable in a hexagonal close packed array after moving them via laser tweezers [20].

The objective of this work is to systematically investigate the propensity for systems of "quadrupole" disks to form a 2D limit-periodic structure. We perform Monte Carlo simulations to identify equilibrium phases at different temperatures of a set of models in which two parameters are varied: (1) the distance, δ, of the embedded charges from the center of each disk; and (2) the set of possible orientations of any given disk. In all cases, the disks are assumed to be pinned to the sites of a triangular lattice. We consider three sets of possible orientations of a given disk. (Note that rotation by π leaves the disk invariant.) In the set R3, the disk may adopt any of the three distinct orientations related by rotation by $\pi/3$. In the set R6, the disk may adopt

any of the six orientations related by rotation by $\pi/6$. And in the set R∞, the disk may rotate continuously.

Highlights of our results include the following. The only rotational move set for which the limit-periodic structure forms is R3. Specifically, we have observed ordering of the first four levels through a sequence of transitions as we slowly lower the temperature of the system. The transitions occur at the same scaled temperature, T_n/E_n, where E_n is the interaction energy of a single disk with all the disks in the same level, n, up to the cutoff in the potential. Simulations using R∞ form level-1 at large values of δ, but are unable to form level-2. Instead the disks that are not part of level-1 (termed "rattlers") all align along a single direction as the temperature is further lowered. Simulations using R∞ at small values of δ are dominated by the formation of a "striped phase" in which the disks in a given stripe all have the same orientation, with that orientation alternating on successive stripes between being along the stripe and perpendicular to it. The simulations using R6 form level-1 order with rattlers aligning in the striped phase at high values of δ; at low values of δ the entire system forms the striped phase.

II. MODEL AND METHODS

An individual disk in our simulations has diameter ζ and is decorated with four point charges of alternating sign at identical distances, δ, from the center of the disk as shown in Fig 2. With the disk in an orientation specified by an angle α, negative charges are placed at positions $\pm\delta\left[\sin(\alpha-\pi/6),\cos(\alpha-\pi/6)\right]$, and positive charges at $\pm\delta\left[\sin(\alpha+\pi/6),\cos(\alpha+\pi/6)\right]$ where the numbers inside the square brackets refer to the x- and y- coordinates of the charges in a body centered reference frame respectively. The disk in

Fig. 2 is shown in the reference configuration $\alpha = \pi/3$. The angles constructed by a pair of neighboring charges and the center of the disk therefore remain fixed and are equal to $\theta = \pi/3$ (where θ is twice the angle between the disk axis in Figure 2 and an individual charge) or equal to $\phi = 2\pi/3$ (where ϕ is twice the angle between the vector perpendicular to the disk axis and an individual charge). The back face of our particle has a reverse "chirality" to the one shown in Figure 1b, but we restrict our simulations to 2D, not allowing disks to flip over and thus ensuring that all retain the same single chirality at all times. Additionally of note is that the net charge and net dipole moment of the disk are both zero. The centers of the disks are taken to be fixed at the positions of a triangular lattice with one basis vector lying in the horizontal direction; translations of the disks are not allowed.

We perform Monte Carlo (MC) simulations for various values of δ and choices of the rotational move set allowed for each individual disk. We study values of δ ranging from 0.05ζ to 0.45ζ in increments of 0.05ζ. A move in our MC simulation consists of a rotation about the center of an individual disk. Three move sets are investigated: (R∞) continuous rotation, (R6) rotation in $\pi/6$ increments; i.e. $\alpha = n\pi/6$ for all integers n, and (R3) rotation in $\pi/3$ increments; i.e. $\alpha = n\pi/3$. The interaction between the charges on separate disks is modeled by an attractive Yukawa potential for charges of unlike sign and a repulsive Yukawa potential of the same magnitude for charges of like sign:

$$U\left(r^*\right) = -\varepsilon q_1 q_2 / r^* \exp\left(-\kappa^* r^*\right) \tag{1}$$

In this equation, ε is a constant with units of energy per charge squared, q_1 and q_2 are the two interacting charges, $r^* = r/\zeta$ where r is the separation distance between the charges, and $\kappa^* = \kappa/\zeta$ where κ is the inverse Debye length. The majority of our simulations use $\kappa^* = 1.194$

and $\varepsilon = 0.113$, which yields $U\left(r^*\right) = -1.0$ at $r^* = 0.1$ and $U\left(r^*\right) = -10^{-6}$ at $r^* = 8.0$. All interaction energies between charges are included up to a cutoff distance $r^* = 8.1$. We refer to this potential as P_1. P_1 is representative of a particle of size $\zeta = 0.36\,\mu\text{m}$ in a solution with a salt concentration of 10^{-6} M [21]. We also perform simulations on a shorter range interaction potential with $\kappa^* = 5.695$, $\varepsilon = 0.177$ and a cutoff at $r^* = 2.1$; we refer to this potential as P_2. P_2 is representative of a particle of size $\zeta = 1.73$ μm in a solution with a salt concentration of 10^{-6} M [21]. The centers of the disks in our simulations are constrained to lie on a triangular lattice, thus the only degree of freedom for a given disk is its orientation α.

We base our potential energy cutoff on the distance between disk centers. All charges on a pair of disks are included (or omitted) in potential energy calculations if the centers of the disk pair are within (or outside) a certain cutoff. The nearest neighbor distance between disk centers of the same level is $2^{n-1}\zeta$ where n is the level number, meaning that level-4 disks have a minimum distance of 8ζ between them. The cutoff at 8.1ζ thus includes interactions between the disks that are nearest neighbors in the level-4 structure. Due to our use of a finite cutoff, levels higher than level-4 cannot form and the disks in these levels will remain disordered. The limit-periodic structures found via our simulations are therefore approximants to the true limit-periodic structure. A potential with a cutoff of at least $2^{n-1}\zeta$ should be able to observe up to level n.

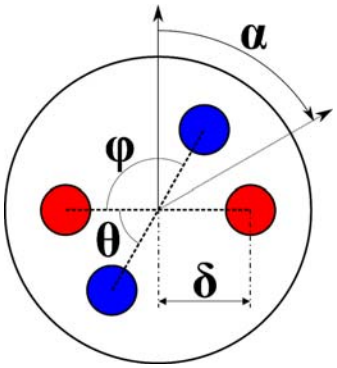

FIG. 2. Quadrupole disk model used in simulations where blue circles (located northeast and southwest on the disk) represent negative point charges and red circles (located east and west on the disk) represent positive point charges. θ and ϕ refer to fixed angles while δ refers to the distance between the center of the disk and a charge. The orientation of the particle is defined by the angle α, which for the orientation shown is equal to $\pi/3$. The orientation is therefore positive for clockwise rotations and negative for counterclockwise rotations.

Our simulations are performed in a rectangular simulation box with periodic boundary conditions in both the x and y directions. The width and length of the simulation box were chosen to accommodate a triangular lattice with lattice constant ζ with periodic boundary conditions. The triangular lattice contains a specified number of rows with each row having the same number of lattice points as there are rows in the system. We refer to the size of these lattices and therefore the system size as n x n where n is the number of rows in a lattice or equivalently the number of lattice points in a single row. The two system sizes investigated were 64×64 and 32×32. The larger system is the same system size as that investigated by Byington et al. and Marcoux et al. and allows for up to level-4 order to be formed [1,11]. We use the larger system size for all the discrete rotation simulations (R6 and R3) as well as for a single continuous rotation simulation (R∞) at a δ value of 0.35. The smaller system size is used for the majority of the continuous rotation simulations since they take considerably longer to perform than the discrete cases. This is because the infinite number of possible disk orientations precludes the use of a potential lookup table (explained below). We simulated 3×10^4 MC cycles at each temperature step for the R3 case, 6×10^4 MC cycles for the R6 case and, 12×10^4 cycles

for the R∞ case. A single cycle consists of 64^2 (the number of disks in the large systems) individual rotational moves. We greatly sped up our discrete rotation simulations by constructing lookup tables for the potential between pairs of disks located at the discrete set of possible relative positions and orientations. Without the speedup afforded by this method it would be computationally difficult to simulate diverse sets of parameters in a reasonable amount of time. For the continuous case, where no lookup table was used, it took approximately 2.94 hours to simulate 10^4 cycles (where one cycle includes an attempted rotational move for each particle in the system) running on nine CPU threads using OpenMP. For the R3 case, where a lookup table was used for the same size system, the same number of cycles took approximately 3.27 minutes running on a single CPU thread.

We chose to use simulated annealing to observe the formation of successive levels of limit-periodic structures. The temperature of the system was lowered in discrete steps, allowing time for equilibration at each step [22]. If a limit-periodic phase is to emerge, increasing levels of order are expected to form as the temperature is lowered. The level-1 lattice will form at a temperature at which the rest of the disks remain free to rotate; these freely rotating disks are referred to as "rattlers". At a lower temperature the level-2 lattice will form. The transitions can occur for a given level ω as long as the cutoff distance for the potential exceeds $2^{\omega-1}\zeta$.

The degree of order for a given individual level of the limit-periodic structure is characterized by the staggered tetrahedral order parameter ϕ_n introduced by Byington and Socolar [1]. When level n orders, the orientations of three fourths of the disks are locked in while that of the one fourth that remain rattlers are not. The rattlers can occupy any of four equivalent sublattices (A, B, C or D in Figure 3a); ϕ_n must allow for any of these four possible modes of ordering. ϕ_n is derived from a sum over all the disks of spin vectors assigned to the

disks to represent their orientations and the sublattice on which each disk sits (i.e. to determine ϕ_n, the orientation and sublattice of each disk must be known). These spin vectors are shown in Figure 3b as arrows which point from the center of a tetrahedron to one of the four possible vertices. At level *n*, each disk j contributes a spin $\boldsymbol{\sigma}_{n,j} = \boldsymbol{e}_X$, where $\boldsymbol{e}_X$ is a unit vector pointing from the center of a 3D tetrahedron shown in Figure 3b towards an individual vertex, $X \in \{A, B, C, D\}$. The letters at the vertices of the tetrahedrons in Figure 3b are also used to label the spin vectors ($\boldsymbol{e}_A$, $\boldsymbol{e}_B$, $\boldsymbol{e}_C$ or $\boldsymbol{e}_D$). Although not explicitly indicated, the four spin vectors are also the same for each tetrahedron and so label A always refers to the upper left vertex of the tetrahedron in Figure 3b, label B to the lower left of the tetrahedron, and so on. Four spin vectors are used because there are four equivalent ways for level n to order, each corresponding to having the rattlers on a unique sublattice. A tetrahedron is used because in the calculation of ϕ_n it is important that the dot product between any spin vector and another spin vector in a different direction always take the same value. In the ordered configuration, the orientation of a given disk depends only on the sublattice on which it sits for non-rattlers; therefore, the spin assigned to it must correspond to its sublattice. The sublattice of a disk determines which of the four tetrahedrons to refer to in Figure 3b as indicated by the letter shown at one of the tetrahedron's vertices. For example, if the disk of interest is on sublattice B, the tetrahedron in the upper right of Figure 3b is referred to. The orientation of the disk then determines which spin vector to pick. For example, for a disk sitting on the D sublattice, which is oriented northwest (i.e. $\alpha = -\pi/3$), the bottom right tetrahedron in Figure 3b would be used and the spin vector assigned to the disk would be $\boldsymbol{\sigma}_{n,j} = \boldsymbol{e}_A$ (the vector pointing in a northwest direction in Figure 3b). The average total spin for the system is calculated as $\boldsymbol{\sigma}_{n,tot} = \sum \boldsymbol{\sigma}_{n,j} / N_n$, where N_n is the total number of disks in

level n and the sum is over all the disks, j, in level n. ϕ_n is then defined as $(3/2)\max\left[\boldsymbol{e}_X \cdot \boldsymbol{\sigma}_{n,tot}\right]$ where $\boldsymbol{e}_X$ runs over all four tetrahedral unit vectors. With this definition, ϕ_n is equal to unity if and only if three of the sublattices have orientations consistent with a level of the limit-periodic structure, regardless of the orientation of the fourth sublattice. In that case, the spin vectors on the three ordered sublattices are all in the same direction (i.e. $\boldsymbol{\sigma}_{n,j}$ is the same for all disks on the ordered sublattices), providing a total contribution of $3/2\times3/4\times1=9/8$ to ϕ_n. The projection of the rattler spins on that spin vector is equal to $-1/3$, independent of the disk's orientation, meaning that all of the rattlers provide a total contribution of to ϕ_n resulting in ϕ_n equal to unity.

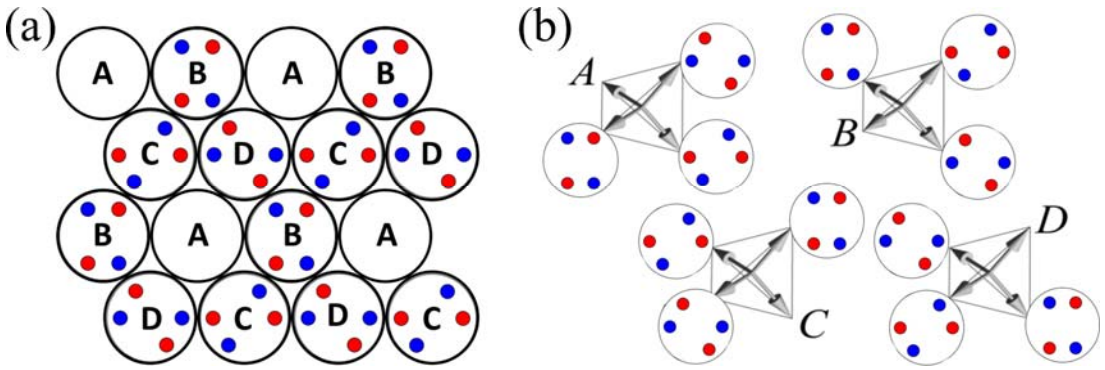

FIG. 3. (a) Sublattice labeling with level-1 ordering shown in which sublattice A contains rattlers whose orientations are not shown. (b) Mapping used to define the value of $\boldsymbol{e}_X$ for an individual disk based on its orientation (north i.e. $\alpha=0$, northwest i.e. $\alpha=-\pi/3$ or northeast i.e. $\alpha=\pi/3$) and sublattice (A, B, C or D) (Figure adapted from Ref [11]). The sublattice of a disk defines which of the four tetrahedrons to use in calculating ϕ_n while the orientation at the end of a vector arrow defines the spin vector for an individual disk. The 3D arrows shown inside the tetrahedrons are the four possibilities for the unit spin vector $\boldsymbol{e}_X$.

This order parameter can be used to characterize successive levels of the limit-periodic structure since the particles on the unordered sublattice (the rattlers) after the system forms a given level n are also in a triangular lattice arrangement which has the ability to form level $n+1$. After level $n+1$ forms, ϕ_{n+1} can be calculated by considering only the particles that were rattlers in level n. This order parameter can be used directly for R3 simulations, but not for R∞ or R6

simulations since ϕ_n is not defined when the orientation of the particle is at values other than $n\pi/3$. For these simulations, the orientation angle is rounded to the nearest value of $n\pi/3$ and then ϕ_n is calculated. When the angle is a multiple of $\pi/6$ but not of $\pi/3$ (which occurs often in the R6 simulations) we randomly choose the orientation angle to be either of the two angles it is halfway between.

We define an additional order parameter for the striped phase that we observe in our R∞ and R6 simulations. The stripes can either involve all of the disks in the system, as in Figure 4a or the first image in Figure 5, or just the rattlers, as in the second image in Figure 5. Following similar reasoning as in the above discussion of ϕ_n, we find that the ordering can be described by a staggered octahedral spin vector, $\boldsymbol{\sigma}_{n,j} = \boldsymbol{e}_X$, where $\boldsymbol{e}_X$ is now a unit vector pointing towards an individual vertex, $X \in \{A_{oct}, B_{oct}, C_{oct}, D_{oct}, E_{oct}, F_{oct}\}$, of a 3D reference octahedron as in Figure 4b. The striped phase can either apply to all of the disks in the system as in Figure 4a or in the first image in Figure 5, or just to the rattlers as in the second image in Figure 5. A staggered octahedral spin vector, $\boldsymbol{\sigma}_{n,j} = \boldsymbol{e}_K$, for each disk j in the system must be measured where n is the level and $\boldsymbol{e}_K$ is a unit vector pointing towards an individual vertex, K, of a 3D reference octahedron as in Figure 4b and can therefore be indicated by a unit vector along one of the three Cartesian axes in 3D. $\boldsymbol{\sigma}_{n,j}$ is calculated based on a disk's orientation (which can be at a rotation angle of $n\pi/6$) and the identity of the sublattice, j, on which it sits according to the diagram in Figure 4b. For example, a disk sitting on the D sublattice with an orientation of $\alpha = 5\pi/6$ would be assigned $\boldsymbol{\sigma}_{n,j} = \boldsymbol{e}_Y$. The average total spin is again defined as $\boldsymbol{\sigma}_{n,tot} = 1/N_n \sum_j \boldsymbol{\sigma}_{n,j}$, where N_n is the total number of disks in the system and the sum is over the whole system. The final order

parameter is defined as $\psi_n = \max\left[\boldsymbol{e}_K \cdot \boldsymbol{\sigma}_{n,tot}\right]$ where $\boldsymbol{e}_K$ runs over all six unit vectors in the reference octahedron in Fig 4b.

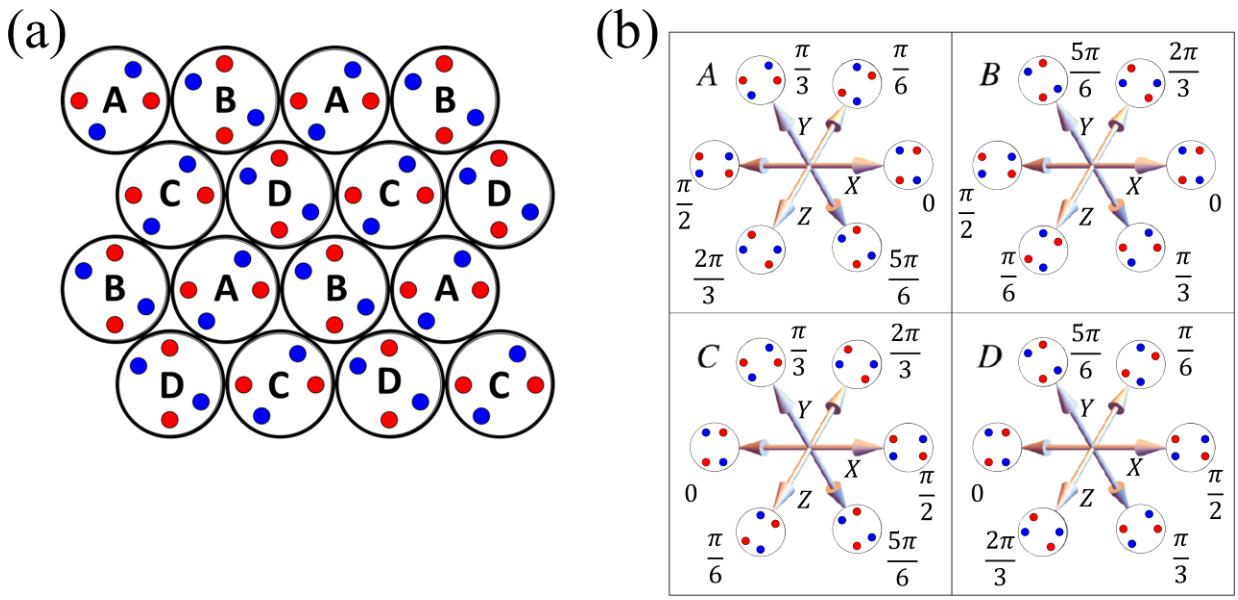

FIG. 4. (a) Sublattice labeling with striped phase shown. (b) Mapping used to define the value of e_K for an individual disk based on its orientation and sublattice (A, B, C or D). The 3D arrows shown inside the octahedrons are the six possibilities for the unit vector $\boldsymbol{e}_K$.

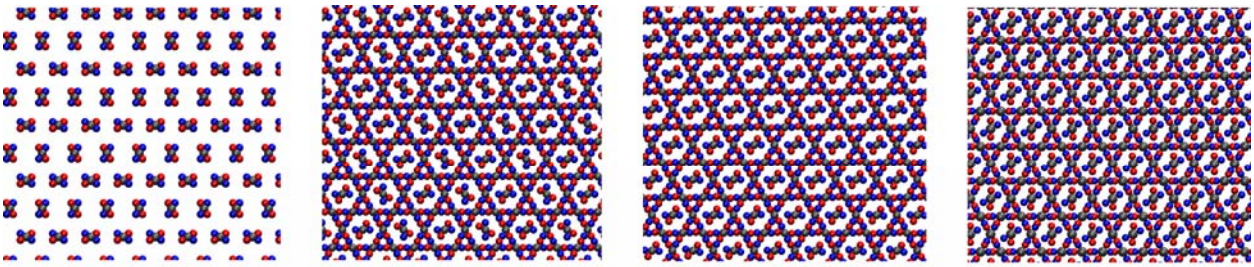

FIG. 5. Images of some of the non-limit-periodic-structures found in our simulations. The gray spheres represent the excluded area of the disk but are shown at reduced size to better visualize the orientation of the disks. Striped phases have alternating bands of disks whose order is determined by the striped order parameter. These stripes can also occur for just the rattlers as shown in the second image. The unidirectional rattler phase is investigated by first measuring ϕ_1 on the entire system and then calculating the nematic order parameter on the rattlers.

A third order parameter is used to measure the occurrence of a nematic-like phase in which the disks not forming the level-1 structure (the rattlers) all align in the same direction as shown in the two figures on the right of Figure 5. The order parameter for these aligned disks is

taken as the 2D nematic order parameter where the global director is determined by the eigenvector associated with the largest eigenvalue of the Q-tensor. The Q-tensor in 2D is defined to be $\frac{1}{N}\sum_{i=0}^{N} 2\boldsymbol{u}_{i\alpha}\boldsymbol{u}_{i\beta} - \delta_{\alpha\beta}$ where $\boldsymbol{u}_i$ is a unit vector which points in the direction of the disk, $\delta_{\alpha\beta}$ is the Kronecker delta, N is the number of disks in the system and α and β run over both x and y components [23]. The largest eigenvalue is the value of the 2D nematic order parameter.

III. RESULTS AND DISCUSSION

One interesting aspect of our model is that the potential energy of a single rattler interacting with its nearest neighbors in the level-1 ordered pattern is independent of the orientation of the rattler. This can be shown by first investigating a single rattler with its six nearest neighbors (which form the level-1 structure around the rattler) as in Figure 6. The potential energy of this rattler with respect to its nearest neighbors is zero because the distances between the charges on the rattler and the charges on neighboring disks multiplied by the sign of the interaction, i.e. $\mathrm{sgn}\left[U\left(r_{ij}\right)\right] * r_{ij}$, cancel out pairwise. There are up to 24 unique pairs of these distances for the rattler; four of the distances which cancel out are shown in Figure 6 (left) where dashed lines of the same color represent equal distances. These distances are equal because, using the indexing in Figure 6, the charged bead 0 on disk 6 and the entirety of disk 0 can be transformed into charged bead 1 on disk 6 and the entire disk 1 by a counter-clockwise rigid rotation of $\pi/3$ about the center of disk 6. Since this is a rigid rotation, the distances between the charges on the rattler and the surrounding disks are maintained. The sign of charges 0 and 1 on the rattler are opposite, which results in an exact cancelation of these contributions to the energy. The other 20 pairs of signed distances arise from a similar analysis for each disk surrounding the

rattler and for charges 2 and 3 on the opposite side of the rattler. This same analysis can be extended to the entire level-1 structure which has formed surrounding the rattler. That is, the whole system can be rotated about the center of an individual rattler by an increment of $\pi/3$ and all levels of a lower index than the rattler will be indistinguishable from their pre-rotated state. We have also measured the potential energy between disks of different levels in the limit-periodic structure formed during our simulations and have found it to be less than 10^{-16}.

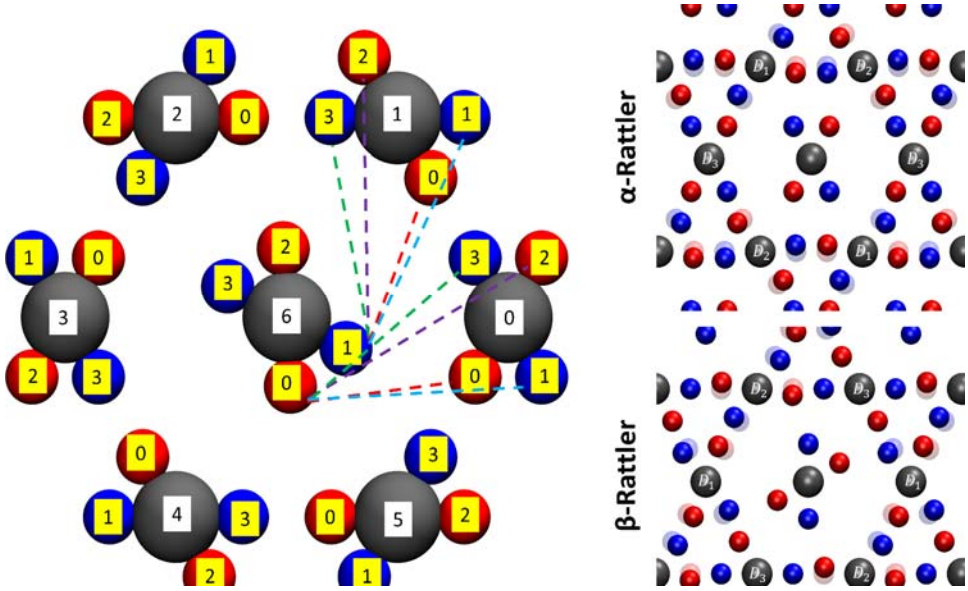

FIG. 6. Left: Image of a rattler (disk 6) and its surrounding six disks (disks 0-5) which are in a Kagome lattice configuration. Regardless of the orientation of the rattler, its potential energy of interaction with the surrounding six disks is zero. The dotted lines show four of the distances which cancel out pairwise according to the color of the lines (colors are the same for lines ending on charges of the surrounding disks with the same number). Right: Images showing the distortion of the rattlers in the α-rattler and the β-rattler phases with the perfectly aligned level-1 structure shown behind transparently. D_1 and D_2 refer to the two sublattices which contain disks which are rotated off of their level-1 structure while D_3 is the non-distorted sublattice.

Since the individual levels of the limit-periodic structure do not interact with each other for our model, it can be helpful to define a scaled δ for predicting how rattlers created during a transition will order upon further decrease in the temperature. The disks in level n are separated by a distance $2^{n-1}\zeta$. For example, the distance between disks in level-3 is 4ζ. All distances associated with a group of disks in the same level can be rescaled by dividing by this distance. In the absence of screening, this results in a rescaled value for delta:

$$\delta_{eff} = \delta / 2^{n-1} \tag{2}$$

δ_{eff} can be used to predict and explain the structure that a given level will form. The rattlers are effectively isolated from the disks in lower levels of the limit-periodic structure. This means that the rattlers should act as an effective system identical to the original one but with $\delta = \delta_{eff}$. The limit-periodic structure will form if and only if the level-1 structure forms for arbitrarily small δ. If the level-1 ordering requires δ above some threshold, δ_c, then the remaining rattlers at sufficiently high levels for which $\delta_{eff} < \delta_c$ will not undergo the required transition and a complete limit-periodic structure will not form.

We begin by describing our results for the simulations using the R∞ moveset, i.e. continuous rotations). The majority of these simulations were performed using a simulation box containing 32 x 32 disks using potential P_2, however we performed one continuous rotation simulation containing 64 x 64 disks using potential P_1 at a δ of 0.35 to ensure that finite size effects were negligible. Each rotational move lies in the range of $[0,\pi]$ with a uniform probability, allowing the disk to adopt any possible orientation in each move. The continuous rotation simulations result in a striped phase at values of $\delta \leq 0.20$ as in the leftmost image of Figure 5. The striped order parameter ψ_1 for this transition versus $\log\left(T^*\right)$ is shown below in Figure 7a. These curves appear to have two distinct regions: one in which the transition is shaped like a tanh function and one in which it is linear before plateauing to a value of 1.0 at low T^*. At values of δ between 0.25 and 0.35 the system forms a unidirectional rattler phase of the type shown in the third image in Figure 5. The order parameters for the systems in this range are shown in Figure 7b where ϕ_1 is indicated by the solid symbols and lines, and the nematic order

parameter of the rattlers is indicated by the open symbols and dashed lines. The orientation of the rattlers in this phase is an integer multiple of $\pi/3$ (i.e. the rattler is parallel to one of the three disk types composing the limit-periodic structure) and so we further specify this phase as a unidirectional α-rattler phase. We display $\delta = 0.25$ on both plots in Figure 7 because at low temperatures it has relatively high values of both ϕ_1 and ψ_1, which we take to mean that this system is a mixed state between the striped phase and the α-rattler phase. This is possible because the transformation of a striped phase to a unidirectional α-rattler phase can be achieved by alternating clockwise and counterclockwise rotations by $\pi/6$ of the disks in the parallel stripe. This rotation angle can be less than $\pi/6$, leading to a mixed phase. The amount of mixing between the two phases decreases as the value of δ increases and the structure becomes more like an ideal unidirectional α-rattler phase. ψ_1 for $\delta = 0.25$ also plateaus to a value around 0.5 at intermediate temperatures and then achieves a relatively high value at lower temperatures suggesting that this temperature is close to the transition between the striped and α-rattler phase. At $\delta \geq 0.40$ the system forms a structure similar to the α-rattler phase except the orientation of the rattlers is $\alpha \in \{\pi/6, \pi/2, 5\pi/6\}$ and so we call this phase the unidirectional β-rattler phase as shown in the rightmost image in Figure 5. Interestingly, the sequence of transitions as a function of T^* is reversed for the two order parameters; as the value of δ increases the ϕ_1 transition occurs at increasingly higher temperatures and the nematic transition at increasingly lower temperatures. This is likely due to the fact that as δ increases, the level-1 structure becomes more energetically stable and therefore it becomes more difficult to distort the level-1 structure to form a unidirectional rattler phase.

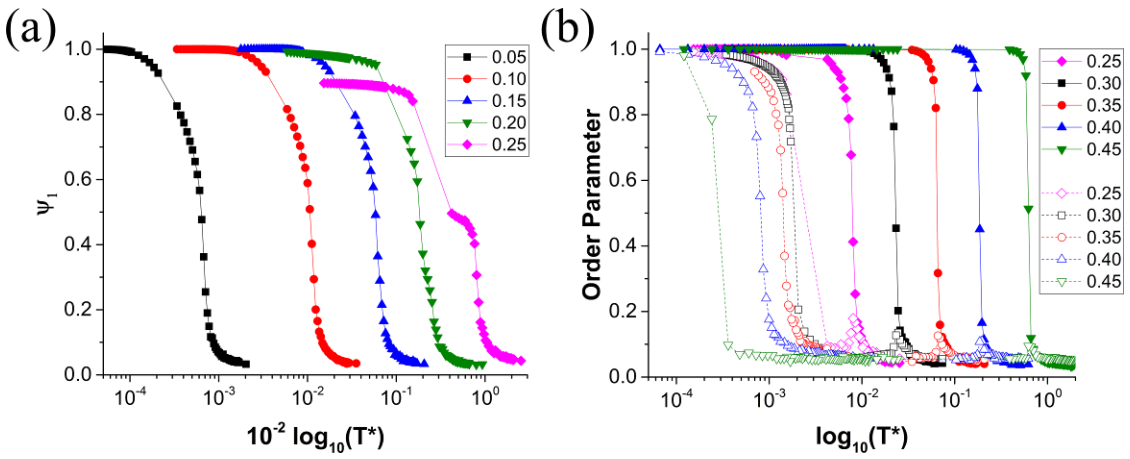

FIG 7: (a) Striped order parameter, ψ_1, versus reduced temperature T^* for continuous rotation simulations. Values of δ are shown in the legend. (b) ϕ_1 (filled symbols and solid lines) and nematic order parameter (open symbols and dashed lines) for continuous rotation simulations. Values of δ are shown in the legend.

The failure of the simulations using R∞ to form level-2 of the limit-periodic structure appears to be due to a distortion in the level-1 structure. This distortion occurs when the disks occupying two of the three sublattices making up the level-1 structure rotate slightly away from an integer multiple of $\alpha = \pi/3$ and their ideal position in a limit-periodic structure. The disks on both the distorted sublattices rotate off their limit-periodic orientation by the same value with one rotating clockwise and the other counter-clockwise. In order to define the distorted sublattices we focus on the level-1 "cage" surrounding a single rattler as in Figure 6 (right). In this "cage" there are two pairs of neighboring disks that are distorted. We refer to the sublattice containing the disk in one of these pairs which is located counterclockwise from its neighboring distorted disk as D_1 and the other sublattice containing the disk located clockwise from its neighboring distorted disk as D_2. For the α-rattler case, the disks on D_1 are rotated clockwise while the disks on D_2 are rotated counter-clockwise as can be seen in the right top image in Figure 6. For the β-rattler case, the reverse is true; the disks on D_1 are rotated counter-clockwise while the

disks on D_2 are rotated clockwise as can be seen in the right bottom image in Figure 6. The exact value of the distortion depends on both the potential and the value of δ with the distortion angle decreasing as δ increases. These distortions cause the level-2 rattler to have a preferred orientation. In the α-rattler phase the preferred orientation of the rattler is $\alpha = \alpha_{D_3}$ where α_{D_3} is the orientation of the disks occupying the non-distorted sublattice of the level-1 structure. For the β-rattler phase $\alpha = \alpha_{D_3} + \pi/2$. All of the level-2 rattlers attain the same orientation at low temperature.

Next we describe the results from simulations using the R6 moveset, i.e. $\pi/6$ rotation simulations. In these simulations, as in the simulations using R∞, a striped phase is present at values of δ less than or equal to 0.25. A plot of the striped order parameter, ψ_1, versus temperature for values of $\delta \leq 0.25$ is shown in Figure 8. All curves show a sharp transition except for the curve at $\delta = 0.25$ which slightly plateaus to a value of 0.3 before it attains a value of 1.0. This system forms a mixed state of level-1 structure and striped phase at around a temperature of 0.01, but upon further lowering of the temperature, the system adopts a purely striped phase configuration. For $\delta \geq 0.30$, the system forms the level-1 structure with rattlers forming a striped phase instead of the level-2 structure. For this case, we first calculate ϕ_1 (to identify which sublattice is the rattler sublattice) and then calculate ψ_2 as shown in Figure 9. For one of our replicates at $\delta = 0.30$ we observe a single system-spanning stripe form while the rest of the system forms the striped rattler phase leading to the large error bars seen for this curve. The rattlers for these simulations do not align in the same fashion as in the continuous rotation simulations due to the fact that in these simulations the level-1 structure cannot distort. Instead the rattlers form a striped phase, as there δ_{eff} is always less than 0.25.

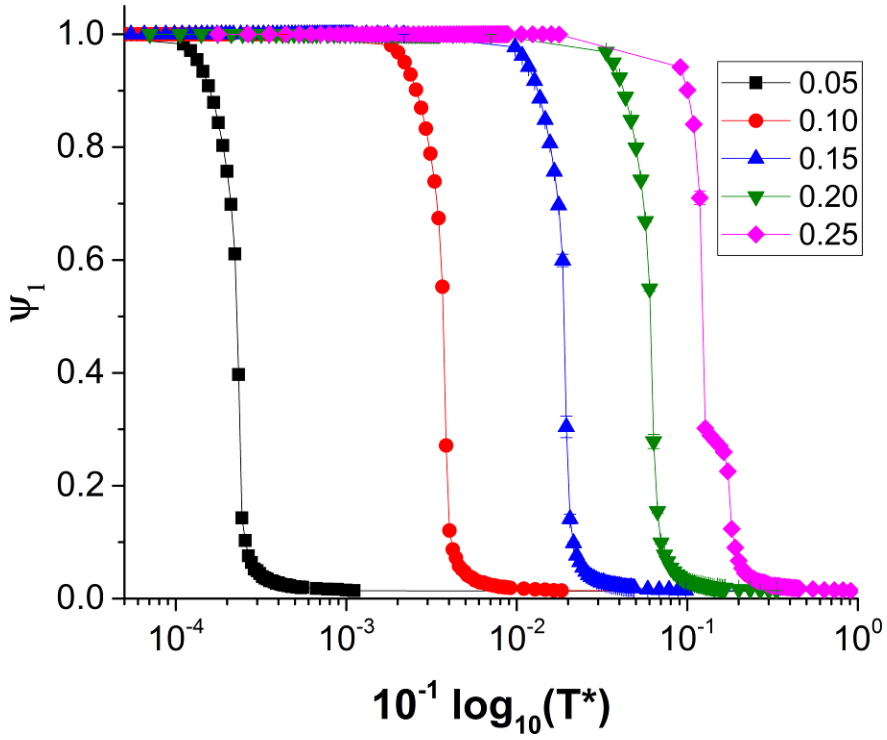

FIG. 8. ψ_1 for $\delta \le 0.25$ using the R6 moveset. Values in the legend indicate the value of δ.

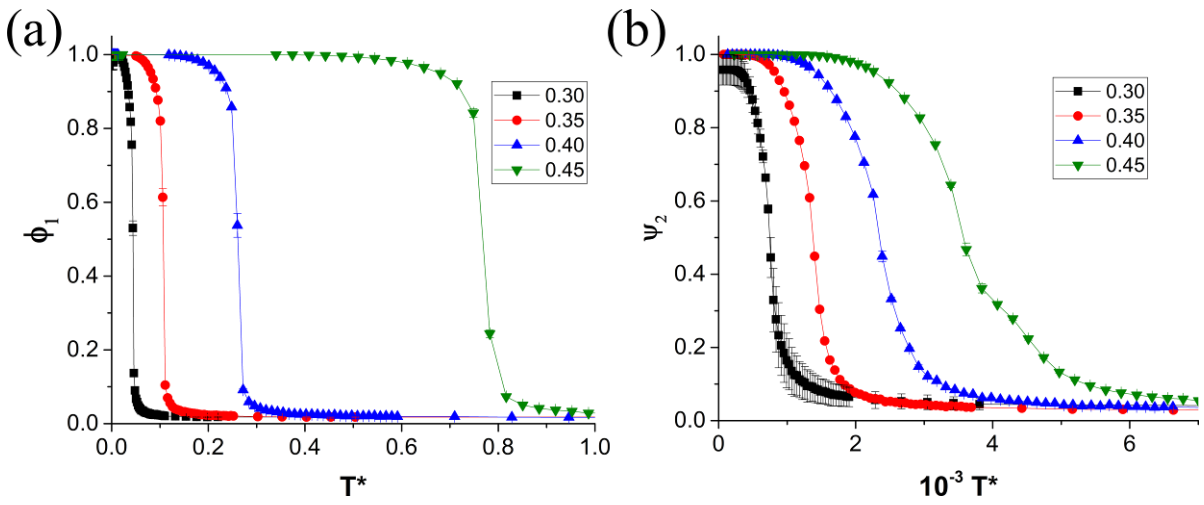

FIG. 9. ϕ_1 (a) and ψ_2 (b) vs. T^* for $\delta \ge 0.30$ using the R6 moveset. Note the difference in the horizontal scales on the two plots. Values in the legend indicate the value of δ.

Finally, we describe our results from simulations using the R3 moveset, i.e. $\pi/3$ rotation simulations. For these simulations, we found that regardless of the value of δ, the limit-periodic

structure forms up to level-4 as shown in the left image of Figure 10. The right image in Figure 10 shows plots of ϕ_n vs. $\log\left(T^*\right)$ for all four of these levels at a single δ of 0.35. The curves are similar to each other except for their transition temperatures and the value of the order parameter at high temperatures which increases with increasing level of order. The dependence of the value of the order parameter at high temperatures on the level appears to be due to a system size effect caused by the number of disks in a given level decreasing as the level increases. We confirm that this split is due to a system size effect by calculating the expected average order parameter at infinite temperature as a function of system size. To do this we randomly select rotations for n disks (as long as n a multiple of four) from the R3 moveset. Randomly selecting the rotations is equivalent to simulating a system at infinite temperature since there are no interactions between the disks. We then calculate ϕ_1 for this imaginary system as a function of the number of disks in the system, N, and fit it to the power law $\phi_1\left(N\right)=1.0175N^{-0.507}$. The value of ϕ_n for each of the four curves in Figure 10 at the highest $\tilde{T}$ simulated, $\tilde{T}_H$, is consistent with the values calculated with this function such that $\phi_n\left(\tilde{T}_H\right)\approx 1.0175\left(64^2\left(1/4\right)^{n-1}\right)^{-0.507}$ where n is the level under consideration. Since the levels do not interact with each other, the curves should collapse if the temperature is divided by the total potential energy for a single disk interacting with other disks in the same level, $U_{a,i-a}$,where a is the level of a single disk, i, interacting with other disks in the same level. We refer to this scaled temperature as $\tilde{T}=T^*/U_{a,i-a}$ and we plot the order parameters for every δ investigated versus $\tilde{T}$ in Figure 11. Scaling the temperature in this manner causes ϕ_n to collapse into four separate curves as a function of $\tilde{T}$, corresponding to the four levels observed in our simulations of the limit-periodic structure. These curves have similar

scaled transition temperatures and merge into a single curve at $\tilde{T}$ values lower than the transition temperature. These curves seem to be associated with continuous phase transitions as they do not have any evidence of hysteresis with temperature. We plot a state diagram showing the different phases formed at the lowest temperatures investigated on a moveset versus δ plane in Figure 12.

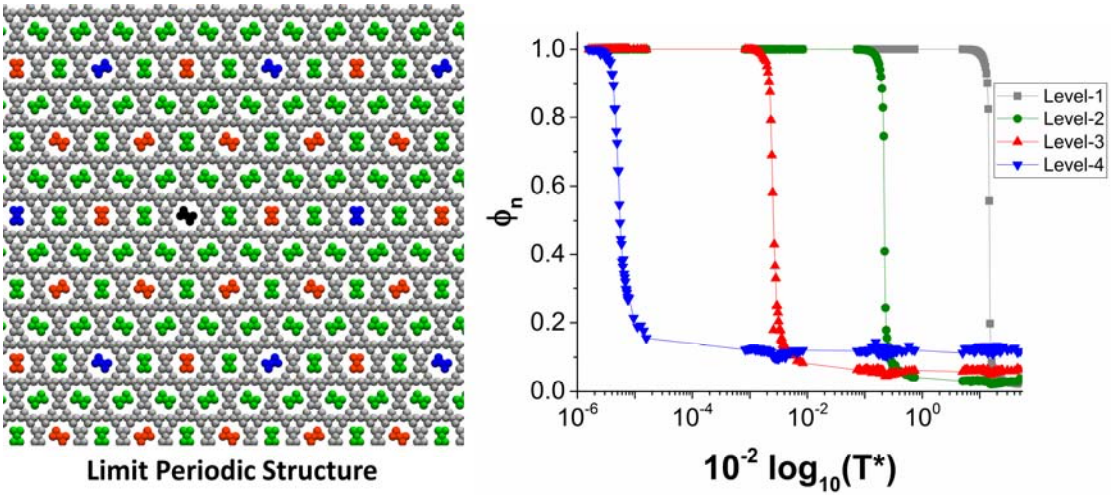

FIG. 10. Subset of the system (22×24 of a 64×64 system) at $\delta = 0.35$ using the R3 moveset color coded according to the level the disks are in. The figure on the right plots ϕ_n for these four levels versus $\log\left(T^*\right)$. In this plot, gray squares correspond to level-1, green circles to level-2, red triangles to level-3 and blue upside-down triangles to level-4. Colors for the image on the left can be seen more clearly in the online version and correspond to the same level as the colors in the figure on the right. Black in the figure on the left is not ordered.

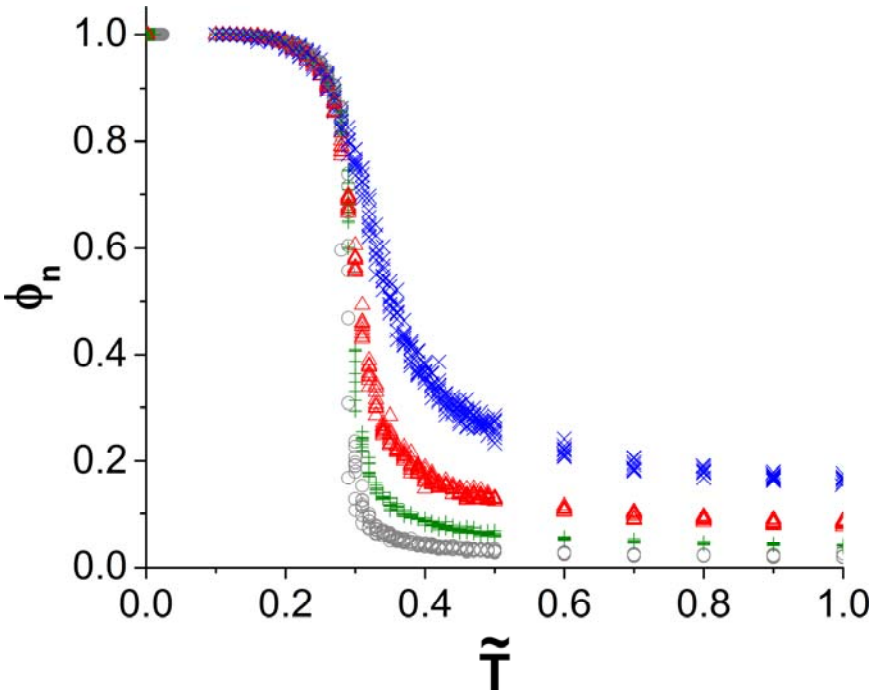

FIG. 11. Order parameters for four levels of order plotted versus $\tilde{T}$ where gray circles are for level-1, green crosses for level-2, red triangles for level-3 and blue x's for level-4.

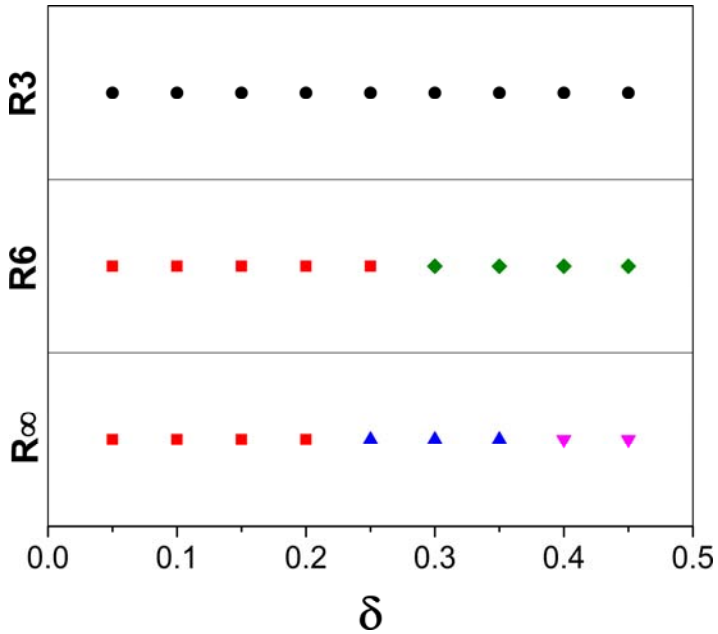

FIG. 12. State diagram showing the different phases found for a given moveset as a function of δ. Red squares stand for striped phase, blue triangles for α-rattler phase, pink upside-down triangles for β-rattler phase, green diamonds for striped rattler phase and black circles for limit-periodic phase.

We have performed exploratory simulations in which we vary θ in our quadrupole model to be either $2\pi/3$, $\pi/2$ or $\pi/18$. Motivation for this comes from the observation that the

location of the point charges does not matter in ensuring the potential energy of the rattler is zero with respect to the surrounding disks. This suggests that other values of θ could also lead to a limit-periodic structure. However, it is not clear if the individual levels of the limit-periodic structure would form for systems with θ other than $\pi/3$. Remarkably, all three systems tested ($\theta = 2\pi/3, \pi/2, \pi/18$) form up to level-4 order through a series of phase transitions similar to the case when $\theta = \pi/3$. Level-4 for each of these systems can be seen in Figure 13. This suggests that θ does not influence whether the system forms the limit-periodic structure. Since δ also does not affect whether the system forms a limit-periodic structure, it may even be possible to form a limit-periodic structure from dipolar disks with an embedded point quadrupole. Even more complex particles may also form the limit-periodic structure since the number of charges on the surrounding six disks also does not matter in ensuring there is no interaction between the levels as long as the number of positive and negative charges on a single disk are equal.

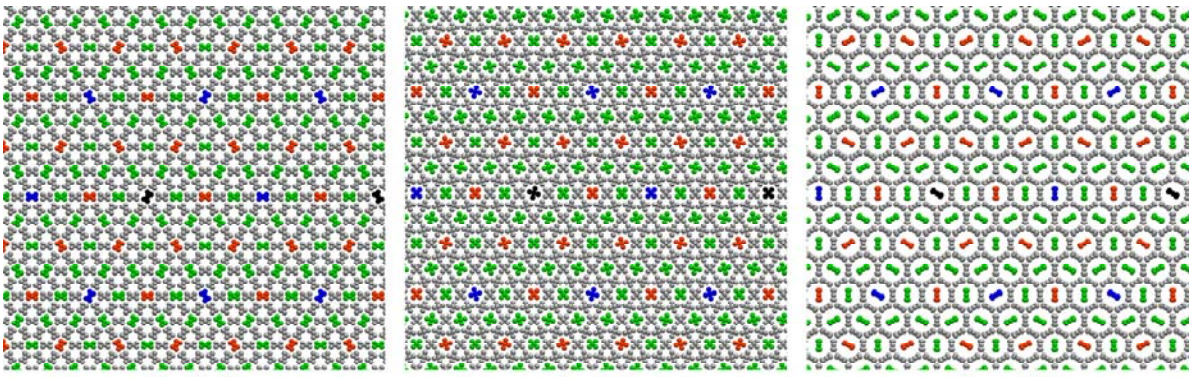

FIG. 13. Images of the structures formed for the quadrupole model at different values of theta; disks are colored the same as in Fig.10. Up to level-4 order is seen in these limit-periodic structures. This suggests that θ does not influence whether the system will form a limit-periodic structure. Colors correspond to the same levels as in Figure 10 and can be more clearly seen in the online version of this manuscript. Disks which are colored black are not ordered.

IV. CONCLUSIONS

We have determined that our quadrupole disk model can form a limit-periodic structure if the rotational moves are limited to $\pi/3$ increments (R3) but not if the rotation moves are either continuous (R∞) or limited to $\pi/6$ increments (R6). Instead the simulations using the R6 moveset form either a striped phase or a striped rattler phase, while continuous rotation simulations form either the striped phase or a unidirectional rattler phase of one of two types. The limit-periodic structure that forms using R3 does not depend on the value of δ or θ and so a wide range of possible particles could be used to create such a structure.

By restricting our simulations to two dimensions (as opposed to confining freely-rotating particles to a plane), the disks adopt a single chirality. The importance of a single chirality for the formation of the limit-periodic structure can be illustrated by an experimental model which is visually very similar to ours that was mentioned briefly by Chen et al. in which four attractive patches were placed on a disk in the same locations as in our model [24]. Instead of forming a limit-periodic structure, these particles were expected to form a Kagome lattice structure. Indeed, in exploratory simulations in quasi-2D, which allows for both chiral states to be interchangeable, we found phases that are consistent with triblock Janus disks including Kagome lattices and hexagonal close packed systems, but not limit-periodic structures. It is only by limiting our system to a single chirality, i.e. by constraining our disks to a 2D plane and disallowing rotation out of plane, that we see the formation of limit-periodic-like order.

The quadrupole disk model differs from the closely related tiling model of Marcoux et al. in two respects. First, the tiling model explicitly includes only nearest neighbor interactions between tiles, while the quadrupole disk model includes interactions between all pairs of disks within the cutoff range. While the formation of higher level structures in the tiling model occurs through effective long range interactions mediated by chains of direct nearest neighbor

interactions, the ordering of rattlers in the quadrupole disk model relies on direct interactions between disks separated by distances corresponding to the lattice constants of the higher level lattices. Second, our model naturally allows for investigation of the effects of continuous rotations. Continuous rotations in both lattice and off lattice simulations have been investigated previously using a model similar to the black stripe model in which six point dipoles are embedded within a sphere. Limit-periodic structure transitions were observed with that model [12].

The question arises as to whether or not our model, which forms the limit-periodic structures when the rotations are limited to the R3 moveset and disks are monodisperse can be realized experimentally. Limiting rotation to $\pi/3$ could be achieved by making the particles regular hexagons instead of disks. Rotating hexagons would likely be difficult, however, so instead a shape somewhere in between a hexagon and a circle might be required. Since the symmetry in the disks and their placement is required for the potential to cancel out, and this canceling out seems important for the formation of the limit-periodic structure, it may be difficult to form such a structure experimentally using the model we have presented in this paper. Slight differences in the disks or holes in the lattice could disrupt the formation of the limit-periodic structure since the interaction energies between disks falls off rapidly as the level increases. One way to form a triangular lattice is to make a Wigner crystal, which results when isotropically repulsive particles are confined to a small volume or area [12]. This could be achieved with the model used in this paper by adding a charge to the center of each disk and restricting the area of the system to a certain size. Enforcing a single chirality could be dealt with by modifying the model so that vertically oriented dipoles are substituted for the individual charges (vertically up (normal to the plane of the disk) for positive charges and vertically down

for negative charges). For such an arrangement, the particle would have the same chirality even if it was flipped over in three dimensions [12].

The novel aspects of our work include the following. Our limit-periodic structure appears to be unique compared to those observed in earlier work since it forms in part due to the isolation of the individual levels from each other. Additionally, unlike prior tile models which considered potentials including up to next nearest neighbors [1] or nearest neighbors [11] our simulations consider intermediate-ranged potentials similar to work done recently with point dipoles [12]. Our simulations have also found competing structures not reported before in simulations of limit-periodic structures including the striped phases and the α- and β- unidirectional rattler phases. While these represent failures of the limit-periodic structure to form they are interesting in their own right. Finally, our model is a simplification of previous models, in particular the black-stripe model, and formation of a limit-periodic phase using our model demonstrates a greater degree of robustness of the limit-periodic phase than previously reported and adds to the number of models which are known to form a limit-periodic structure.

ACKNOWLEDGMENTS

This work was supported by the Research Triangle MRSEC under grant number DMR-1121107 and the US National Science Foundation under grant OISE 1065466. We would also like to thank Dr. Sabine Klapp for helpful discussions.

REFERENCES

[1] T. W. Byington and J. E. S. Socolar, Phys. Rev. Lett. **108**, 045701 (2012).
[2] C. Janot, *Quasicrystals: a primer* (Clarendon Press; Oxford University Press, Oxford; New York, 1994).

[3] N. A. Wasio, R. C. Quardokus, R. P. Forrest, C. S. Lent, S. A. Corcelli, J. A. Christie, K. W. Henderson, and S. A. Kandel, Nature **507**, 86 (2014).
[4] X. B. Zeng, G. Ungar, Y. S. Liu, V. Percec, S. E. Dulcey, and J. K. Hobbs, Nature **428**, 157 (2004).
[5] K. Hayashida, T. Dotera, A. Takano, and Y. Matsushita, Phys. Rev. Lett. **98**, 195502 (2007).
[6] S. Fischer, A. Exner, K. Zielske, J. Perlich, S. Deloudi, W. Steurer, P. Lindner, and S. Foerster, Proc. Natl. Acad. Sci. U. S. A. **108**, 1810 (2011).
[7] D. V. Talapin, E. V. Shevchenko, M. I. Bodnarchuk, X. Ye, J. Chen, and C. B. Murray, Nature **461**, 964 (2009).
[8] C. Xiao, N. Fujita, K. Miyasaka, Y. Sakamoto, and O. Terasaki, Nature **487**, 349 (2012).
[9] J. Dubois, Chem. Soc. Rev. **41**, 6760 (2012).
[10] *Quasicrystals: an introduction to structure, physical properties and applications*, edited by J.-B. Suck, M. Schreiber, P. Häussler, eds., P. Häussler and J. B. Suck (Springer, Berlin ; New York, 2002).
[11] C. Marcoux, T. W. Byington, Z. Qian, P. Charbonneau, and J. E. S. Socolar, Physical Review E **90**, 012136 (2014).
[12] C. Marcoux Belley, Doctor of Philosophy Duke University, 2016.
[13] R. Berger, *The undecidability of the domino problem*, 1966), p. 1-72.
[14] R. M. Robinson, Inventiones Mathematicae **12**, 177 (1971).
[15] C. Goodman-Strauss, European Journal of Combinatorics **20**, 375 (1999).
[16] J. E. S. Socolar and J. M. Taylor, Mathematical Intelligencer **34**, 18 (2012).
[17] S. Gangwal, A. Pawar, I. Kretzschmar, and O. D. Velev, Soft Matter **6**, 1413 (2010).
[18] S. Gangwal, O. J. Cayre, M. Z. Bazant, and O. D. Velev, Phys. Rev. Lett. **100**, 058302 (2008).
[19] S. Gangwal, O. J. Cayre, and O. D. Velev, Langmuir **24**, 13312 (2008).
[20] M. Skarabot, M. Ravnik, S. Zumer, U. Tkalec, I. Poberaj, D. Babic, N. Osterman, and I. Musevic, Physical Review E **77**, 031705 (2008).
[21] J. N. Israelachvili, *Intermolecular and surface forces* (Academic Press, Burlington, MA, 2011).
[22] A. R. Leach, *Molecular modelling: principles and applications* (Pearson/Prentice Hall, Harlow, England; New York, 2001).
[23] D. G. Barci and D. A. Stariolo, Physical Review B **79**, 075437 (2009).
[24] Q. Chen, S. C. Bae, and S. Granick, Nature **469**, 381 (2011).